Soliton pairs in two-dimensional nonlocal media

Georgios N. Koutsokostas,[1] Theodoros P. Horikis,[2] and Dimitrios J. Frantzeskakis[1]
[1]*Department of Physics, National and Kapodistrian University of Athens, Panepistimiopolis, Zografos, Athens 15784, Greece*
[2]*Department of Mathematics, University of Ioannina, Ioannina 45110, Greece*

(Received 21 January 2020; accepted 20 March 2020; published 16 April 2020)

We study the interaction of optical beams of different wavelengths, described by a two-component, two-dimensional (2D) nonlocal nonlinear Schrödinger (NLS) model. Using a multiscale expansion method the NLS model is asymptotically reduced to the completely integrable 2D Mel'nikov system, the soliton solutions of which are used to construct approximate dark-bright and antidark-bright soliton solutions of the original NLS model; the latter being unique to the nonlocal NLS system with no relevant counterparts in the local case. Direct numerical simulations show that, for sufficiently small amplitudes, both these types of soliton stripes do exist and propagate undistorted, in excellent agreement with the analytical predictions. Larger amplitude of these soliton stripes, when perturbed along the transverse direction, disintegrate either to filled vortex structures (the dark-bright solitons) or to radiation (the antidark-bright solitons).

DOI: 10.1103/PhysRevE.101.042208

I. INTRODUCTION

Solitons, namely, robust localized waveforms that can be formed in nonlinear dispersive media, have been studied extensively in a wide range of physical contexts [1] and in applied mathematics [2]. Furthermore, the so-called vector solitons that emerge in multicomponent settings have been an active area of research due to their relevance in many physical contexts, such as nonlinear optics [3,4], Bose-Einstein condensates (BECs) [5–7], plasmas [8], nematic liquid crystals [9], and so on. One of the most prototypical models that governs the dynamics of such multicomponent solitons is the vector nonlinear Schrödinger (NLS) equation, composed of nonlinearly coupled NLS equations. Variants of the vector NLS have been used, e.g., in optics, to describe the interaction between waves of different frequencies and of the same polarization or of the same frequency but of different polarizations [3]. Coupled NLS equations also appear in the study of BECs, where they model interactions between different spin states of the same atom species, or different Zeeman sub-levels of the same hyperfine level [5,6].

Depending on the nature of inter- and intracomponent interactions [i.e., attractive (focusing nonlinearity) or repulsive (defocusing nonlinearity)], various types of vector NLS solitons may exist, such as bright-bright solitons for focusing nonlinearities, as well as dark-dark or dark-bright solitons for defocusing nonlinearities [3,4]. The latter, namely, dark-bright solitons, are of particular interest, since they occur in defocusing settings, where bright solitons do not exist as solutions of the relative single NLS equation. Nevertheless, the bright soliton component does emerge because of an effective potential well created by the dark soliton through the intercomponent interaction; as such, dark-bright solitons can be thought of as "symbiotic" structures. Dark-bright solitons have been studied extensively in optics, where they were first predicted in the pioneering works Refs. [10,11], as well as in BECs. In both cases, these states have also been observed and studied in experiments (see the review Ref. [7] and references therein), while they have also been predicted to occur in nonlocal nonlinear media [12,13]. In optics, dark-bright solitons have been proposed for applications, where dark solitons could potentially serve as adjustable wave guides for weak signals [3,4,7].

Regarding the type of individual solitons that may couple to form a vector NLS soliton, an interesting possibility is the following: One component of the vector soliton is an antidark soliton, namely, a hump, instead of a dip, on top of the background wave. Antidark solitons where first predicted to occur in single-component NLS models incorporating higher-order effects [14,15] (see also the relevant works Refs. [16,17]), and later they were also found in multicomponent systems. In such settings, the antidark soliton component is usually coupled with a dark soliton—see, e.g., Refs. [18,19] and [20,21] for works in optics and BECs, respectively. However, there is still another possibility, namely, the formation of a vector soliton composed of an antidark and a bright soliton, as was shown in optics [18] and BECs [22]. Notice that antidark-bright solitons, along with dark-bright ones, were recently observed experimentally in weakly birefringent cavity fiber lasers [23]; in this case, however, the experimental setting was relevant to a nonconservative (non Hamiltonian), Ginzburg-Landau-type model, rather than a conservative (Hamiltonian) one, as was the case of the works quoted above.

In this work, we study the formation and dynamics of vector solitons in nonlocal NLS equations, i.e., in a two-component NLS model featuring a nonlocal nonlinearity. Such nonlocal systems arise in a variety of physical settings, including vapors [24,25] and liquid solutions [26,27] exhibiting thermal nonlinearity (see also the review Refs. [28,29]), plasmas [30,31], nematic liquid crystals [9,32–34], dipolar BECs [35], and so on. The model under consideration is generic and it may be used to describe the interaction between two incoherently coupled beams, differing in wavelength (as

in the case of Ref. [10]). Both defocusing and focusing nonlinearities are considered as, e.g., in the case of nematic liquid crystals where the nonlinearity is generally of the focusing type, but it can be made defocusing upon doping the nematic liquid crystals, e.g., with azo dyes [36].

Considering a two-dimensional (2D) setting, we use a multiscale expansion method to show that the system can be reduced to a completely integrable system, namely, the Mel'nikov system in $(2+1)$-dimensions [37]. This system, which was originally introduced to describe the interaction of long waves with short wavepackets [38–40], arises in the description of vector solitons in optics [18] and BECs [41,42]. In our 2D setup, the Mel'nikov system is composed of a Kadomtsev-Petviashvili (KP) equation with a source satisfying a linear Schrödinger equation, and possesses exact analytical soliton solutions. The latter give rise to approximate (small-amplitude) vector soliton solutions of the original nonlocal NLS system, which are found to be of the following type: (a) dark-bright solitons, which are supported in the fully defocusing regime, i.e., when nonlinearities in both components are of defocusing type, and (b) antidark-bright solitons, occurring in the case where the components feature nonlinearities of different types, i.e., defocusing (focusing) for the antidark (bright) soliton component. Interestingly, the first have local NLS counterparts, while the latter are unique to the nonlocal system.

We also perform direct numerical simulations to test the validity of our analytical investigations, and also investigate the stability and dynamics of the derived vector solitons. In particular, we find that small-amplitude solitons of both types (dark-bright and antidark-bright) are quite robust and propagate undistorted in the 2D nonlocal NLS setting, with constant velocity which is correctly predicted by our analysis. Thus, sufficiently weak solitons do exist and are accurately described by our perturbative results. However, we numerically investigate the dynamics of large-amplitude vector solitons, which are perturbed along the transverse direction. We find that, in this case, both soliton types are unstable and are eventually destroyed. The soliton decay occurs earlier for a weak nonlocality, while a stronger nonlocality does prolong the solitons' lifetimes but it is not able to completely suppress the instability. Notice that in the case of dark-bright solitons, the dark soliton component decays into a chain of vortex pairs, filled by 2D, vorticity-free structures that are formed in the bright soliton component. Contrarily, antidark-bright solitons decay into small-amplitude waves.

The paper is organized as follows. In Sec. II, we introduce the model and study the linear regime. In Sec. III, we use a multiscale expansion technique to reduce the model to the Mel'nikov system and derive approximate soliton solutions. In Sec. IV we present our numerical results. Finally, in Sec. V, we summarize our findings and present our conclusions.

II. MODEL AND LINEAR REGIME

We consider the propagation of two incoherently coupled optical beams—generated by different wavelengths, neglecting generation of new frequencies (as, e.g., in the case of Ref. [10])—in a nonlinear medium. Let u and v be the complex electric field envelopes of the two light beams, and the real function n be the nonlinear, generally nonlocal, medium's response, assumed to obey a diffusion-type equation. Then, beam evolution is governed by the dimensionless equations,

$$iu_t + \frac{d_1}{2}\Delta u - 2g_1 nu = 0, \tag{1}$$

$$iv_t + \frac{d_2}{2}\Delta v - 2g_2 nv = 0, \tag{2}$$

$$\nu\Delta n - 2qn + 2(g_1|u|^2 + g_2|v|^2) = 0, \tag{3}$$

where subscripts denote partial derivatives. Here, t denotes the propagation distance (taken to be along the z direction), $\Delta \equiv \partial_x^2 + \partial_y^2$ is the transverse Laplacian, the coefficients $d_{1,2}$ and $g_{1,2}$ characterize, respectively, the diffraction and nonlinearity for the two wavelengths. Notice that (for $d_{1,2} > 0$) the cases with $g_{1,2} < 0$ or $g_{1,2} > 0$ correspond, respectively, to a focusing or a defocusing nonlinearity.

The above system may find applications in a variety of nonlocal media. These include thermal media, such as atomic vapors [24,25] and liquid solutions [26,27] (in this case n is the light intensity-dependent nonlinear change of the refractive index), plasmas (with n being the relative electron temperature perturbation) [30,31], as well as nematic liquid crystals (in this case, n represents the perturbation of the optical director angle from its static value due to the light beams) [9,34]. In this latter context of liquid crystals, the parameter q is related to the square of the applied static field which pretilts the nematic dielectric [32,33]. Finally, the parameter ν describes the strength of nonlocality: large ν corresponds to a highly nonlocal response, while for $\nu = 0$ one obtains the following vector NLS with local cubic nonlinearity:

$$iu_t + \frac{d_1}{2}\Delta u - \frac{2g_1}{q}(g_1|u|^2 + g_2|v|^2)u = 0, \tag{4}$$

$$iv_t + \frac{d_2}{2}\Delta v - \frac{2g_2}{q}(g_1|u|^2 + g_2|v|^2)v = 0. \tag{5}$$

Below, for the purposes of our analysis, we assume that all parameters involved in Eqs. (1)–(3) are positive; an exception refers to the nonlinearity coefficients $g_{1,2}$, which will be allowed to take either positive or negative values, so as to study both the defocusing and the focusing scenarios.

Furthermore, as we are interested in finding solutions of the above system in the form of dark-bright or antidark-bright solitons, we assume—without loss of generality—that the u-(v-)component supports the dark/antidark (bright) soliton. We thus supplement the system Eqs. (1)–(3) with the following boundary conditions:

$$u \to \rho_0 e^{i\phi_0 t}, \quad v \to 0, \quad n \to n_0, \quad \text{as} \quad |x|,\ |y| \to \infty, \tag{6}$$

where ρ_0, ϕ_0, and n_0 are real constants.

To proceed with our analysis, we introduce the Madelung transformation for the field u, namely, $u = \sqrt{\rho}\exp(i\phi)$, where real functions $\rho = \rho(x, y, t)$ and $\phi = \phi(x, y, t)$ denote the amplitude and phase, respectively. Then, Eqs. (1)–(3) reduce

to the following hydrodynamic-type form:

$$\rho_t + d_1 \nabla \cdot (\rho \nabla \phi) = 0, \tag{7}$$

$$\phi_t + 2g_1 n + \frac{d_1}{2}(|\nabla\phi|^2 - \rho^{-1/2}\Delta\rho^{1/2}) = 0, \tag{8}$$

$$iv_t + \frac{d_2}{2}\Delta v - 2g_2 n v = 0, \tag{9}$$

$$v\Delta n - 2qn + 2(g_1\rho + g_2|v|^2) = 0, \tag{10}$$

where $\nabla = (\partial_x, \partial_y)$ is the gradient operator. It can now be observed that the simplest nontrivial solution of the above system, satisfying the boundary conditions Eq. (6), reads

$$\rho = \rho_0, \quad \phi = -2g_1 n_0 t, \quad v = 0, \quad n = n_0 = \frac{g_1}{q}\rho_0, \tag{11}$$

where $\rho_0 = \text{const}$. This solution, which has the form of a continuous wave in component u and the trivial state in component v, will serve as a "background" on top of which we will seek soliton solutions. The stability analysis of the above background solution can be performed upon introducing to Eqs. (7)–(10) the perturbation ansatz:

$$\begin{aligned} &\rho = \rho_0 + \epsilon\tilde{\rho}, \quad && \phi = -2g_1 n_0 t + \epsilon\tilde{\phi}, \\ &v = \epsilon\tilde{v}, && n = n_0 + \epsilon\tilde{n}, \end{aligned} \tag{12}$$

where ϵ is a formal small parameter ($0 < \epsilon \ll 1$), and perturbations $\tilde{\rho}$, $\tilde{\phi}$, $\tilde{v}$, $\tilde{n}$ are $\sim \exp[i(\boldsymbol{k}\cdot\boldsymbol{r} - \omega t)]$ [here, $\boldsymbol{k} \equiv (k_x, k_y)$ and ω are the wave vector and frequency of the perturbation, respectively, and $\boldsymbol{r} \equiv (x, y)$]. Substitution of Eq. (12) into Eqs. (7)–(10) yields—to leading-order in ϵ—the following results.

First of all, Eqs. (7), (8), and (10), which decouple from Eq. (9), lead to the dispersion relation

$$\omega^2 = \frac{4d_1 g_1^2 \rho_0}{2q + \nu k^2}k^2 + \frac{d_1^2}{4}k^4, \tag{13}$$

where $k^2 = k_x^2 + k_y^2$. The above equation shows that if $d_1 > 0$, then $\omega \in \mathbb{R} \forall k \in \mathbb{R}$, i.e., the solution $\rho = \rho_0$, $\phi = -2g_1 n_0 t$, $n = n_0$ is always stable. In this case, and in the long-wavelength limit corresponding to $(\nu/2q)k^2 \ll 1$, the dispersion relation Eq. (13) simplifies to a Bogoliubov-type form:

$$\omega^2 = c^2 k^2 + \frac{d_1^2}{4}\alpha k^4, \quad c^2 = \frac{2}{q}d_1 g_1^2 \rho_0, \tag{14}$$

where c is the "speed of sound," i.e., the propagation speed of small-amplitude long waves propagating on top of the solution Eq. (11), while parameter α is given by

$$\alpha = 1 - \frac{4g_1^2 \nu \rho_0}{d_1 q^2}. \tag{15}$$

As we will see below, the sign (and magnitude) of this parameter controls the type of solitons that can be supported by the system.

Finally, in the same context of the linear regime, Eq. (9) leads to a linear Schrödinger-type dispersion relation,

$$\omega - \frac{d_2}{2}k^2 - 2g_2 n_0 = 0. \tag{16}$$

Obviously, here too, $\omega \in \mathbb{R}$, $\forall k \in \mathbb{R}$, implying that $v = 0$ is stable. We can thus conclude that, as long as $d_1 > 0$, solution Eq. (11) is stable.

III. NONLINEAR REGIME—SOLITON SOLUTIONS

We now proceed by analyzing Eqs. (7)–(10) by means of a multiscale expansion method. This will lead to the derivation of an effective Mel'nikov system [37], the solutions of which will be exploited for the construction of soliton solutions for the original system Eqs. (1)–(3).

Seek small-amplitude solutions on top of the background solution Eq. (11) in the form of the following asymptotic expansions in ϵ:

$$\rho = \rho_0 + \epsilon\rho_1 + \epsilon^2\rho_2 + \cdots, \tag{17}$$

$$\phi = -2g_1 n_0 t + \epsilon^{1/2}\phi_1 + \epsilon^{3/2}\phi_2 + \cdots, \tag{18}$$

$$v = \epsilon Q \exp[i(k_x x + k_y y - \omega t)], \tag{19}$$

$$n = n_0 + \epsilon n_1 + \epsilon^2 n_2 + \cdots, \tag{20}$$

where the unknown fields ρ_j, ϕ_j, n_j (with $j = 1, 2, \ldots$) and Q depend on the slow variables:

$$X = \epsilon^{1/2}(x - ct), \quad Y = \epsilon y, \quad T = \epsilon^{3/2}t, \tag{21}$$

where c is the speed of sound [see Eq. (14)]. Notice that, according to the original boundary conditions Eq. (6), the unknown fields must satisfy ρ_j, ϕ_j, n_j, $Q \to 0$ as $X, Y \to \pm\infty$. Substituting expansions Eqs. (17)–(20) into Eqs. (7)–(10), and using variables Eqs. (21), we obtain the following results. First, Eq. (7) yields

$$O(\epsilon^{3/2}): \quad -c\rho_{1X} + d_1\rho_0\phi_{1XX} = 0, \tag{22}$$

$$\begin{aligned} O(\epsilon^{5/2}): \quad &\rho_{1T} - c\rho_{2X} + d_1[(\rho_1\phi_{1X})_X \\ &+ \rho_0\phi_{1YY} + \rho_0\phi_{2XX}] = 0. \end{aligned} \tag{23}$$

From Eq. (8),

$$O(\epsilon): \quad -c\phi_{1X} + 2g_1 n_1 = 0, \tag{24}$$

$$\begin{aligned} O(\epsilon^2): \quad &\phi_{1T} - c\phi_{2X} + 2g_1 n_2 \\ &+ \frac{d_1}{2}\left(\phi_{1X}^2 - \frac{1}{2\rho_0}\rho_{1XX}\right) = 0, \end{aligned} \tag{25}$$

and Eq. (10) leads to

$$O(\epsilon): \quad -qn_1 + g_1\rho_1 = 0, \tag{26}$$

$$O(\epsilon^2): \quad \nu n_{1XX} - 2qn_2 + 2(g_1\rho_2 + g_2|Q|^2) = 0. \tag{27}$$

Using Eq. (26), it is readily seen that the compatibility condition of the leading-order Eqs. (22) and (24) yields the speed of sound given in Eq. (14). In addition, the compatibility conditions of the nonlinear Eqs. (23) and (25) can be found as follows. Multiply Eq. (23) by $2g_1^2/q$; substitute n_2 from Eq. (27) into Eq. (25), multiply by c and differentiate once with respect to X. Then, adding the resulting equations, and using the definition of the speed of sound, as well as the auxiliary equation $\phi_{1X} = (2g_1^2/qc)\rho_1$ [obtained from Eqs. (24) and

(26)], we find that the compatibility condition of Eqs. (23) and (25) is the following nonlinear equation:

$$\left(\rho_{1T} - \frac{d_1^2\alpha}{8c}\rho_{1XXX} + \frac{3c}{2\rho_0}\rho_1\rho_{1X}\right)_X + \frac{c}{2}\rho_{1YY} + \frac{cg_2}{2g_1}(|Q|^2)_{XX} = 0, \tag{28}$$

where α is given by Eq. (15). Next, we proceed with Eq. (9). To leading-order [i.e., at $O(\epsilon)$], this equation yields the linear dispersion relation Eq. (16), while at $O(\epsilon^{3/2})$ one obtains $k_x = -c/d_2$. Finally, at $O(\epsilon^2)$, we derive the equation

$$iQ_Y + \frac{1}{2k_y}Q_{XX} - \frac{2g_1g_2}{qd_2k_y}\rho_1 Q = 0. \tag{29}$$

Equations (28) and (29) constitute the Mel'nikov system in $(2+1)$-dimensions [37], which is composed of a KP equation with a self-consistent source, which satisfies a Schrödinger equation. This system possesses soliton solutions of the form

$$\rho_1 = -A\,\mathrm{sech}^2\,\xi, \tag{30}$$

$$\begin{aligned}\xi &\equiv K_X X + K_Y Y + \Omega T,\\ Q &= Be^{i\Phi}\,\mathrm{sech}\,\xi,\\ \Phi &= -\frac{K_Y k_y}{K_X}X + \left(\frac{K_X^4 - K_Y^2k_y^2}{2K_X^2k_y}\right)Y,\end{aligned} \tag{31}$$

where the soliton amplitude A is given by

$$A = \frac{1}{c^2}d_1^2K_X^2\rho_0\alpha, \quad \rho_0 = \frac{d_1q^2}{4\nu g_1^2}(1-\alpha), \tag{32}$$

with the requirement $\alpha < 1$ so that $\rho_0 > 0$. In addition, the real parameters K_X, K_Y, and Ω, as well as the (generally complex) amplitude parameter B are connected through the equation

$$-c\left(cK_Y^2 + 2K_X\Omega\right) + d_1^2\alpha\left(K_X^4 + 4\rho_0B^2\frac{g_1g_2^3}{d_2^2q^2}\right) = 0. \tag{33}$$

The solution Eqs. (30) and (31) of the Mel'nikov system can now be used to construct solitons of the nonlocal system Eqs. (1)–(3). Indeed, approximate soliton solutions, valid up to order $O(\epsilon)$, can be found upon using at first Eqs. (24) and (26) to express n_1 and ϕ_1 in terms of ρ_1:

$$n_1 = \frac{g_1}{q}\rho_1, \quad \phi_1 = \frac{2g_1^2}{qc}\int \rho_1(X')dX'. \tag{34}$$

Then, the approximate soliton solution of Eqs. (1)–(3) reads

$$u \approx (\rho_0 - \epsilon A\,\mathrm{sech}^2\,\xi)^{1/2} \times \exp\left[-2i\left(g_1n_0t + \epsilon^{1/2}\frac{g_1^2}{qcK_X}A\tanh\xi\right)\right], \tag{35}$$

$$v \approx \epsilon B\,\mathrm{sech}\,\xi\,\exp[i(k_xx + k_yy - \omega t + \Phi)], \tag{36}$$

$$n \approx n_0 - \frac{g_1}{q}\epsilon A\,\mathrm{sech}^2\,\xi. \tag{37}$$

It can readily be observed that Eq. (36) describes a sech-shaped bright soliton, while Eq. (35) describes two different types of solitons, namely, dark or antidark ones, for $A > 0$ and $A < 0$, respectively: indeed, if $A > 0$ ($A < 0$), then the solution has the form of a density dip (hump) on top of the background solution $(u, v) = [\rho_0^{1/2}\exp(-2ig_1n_0t), 0]$. It is important to point out that the sign of A depends on the sign (and magnitude) of the parameter α. In particular, as indicated by Eq. (32), if $0 < \alpha < 1$ the soliton in the u-component is dark, while for $\alpha < 0$ or $\alpha > 1$ it is antidark. These requirements are satisfied as long as $g_2 > 0$ and $g_2 < 0$, respectively, which means that the dark-bright solitons are formed for $g_1 > 0$ and $g_2 > 0$, while antidark-bright ones are supported when $g_1 > 0$ and $g_2 < 0$ (see also discussion below).

It is also relevant, at this point, to discuss the role of nonlocality on the type of the vector solitons that can be formed. For this purpose, let us consider the local limit, with $\nu \to 0$. In this case, according to Eq. (15), the parameter α becomes independent of ν, and takes only the constant value $\alpha = 1$. Then, the dark soliton component's amplitude is given by the first of Eqs. (32) (the second of Eqs. (32) is now an identity), while the amplitude B of the bright soliton component is given by Eq. (33), with $\alpha = 1$ and with ρ_0 being a free parameter. Thus, in the local limit, one has always $A = (1/c^2)d_1^2K_X^2\rho_0 > 0$, regardless of the sign of g_2; this means that, in this limit, *only* dark-bright solitons are possible. Hence, antidark-bright solitons can only be supported by the nonzero nonlocality, i.e., $\nu \neq 0$, and are unique to this system without any local counterparts.

IV. NUMERICAL SIMULATIONS

We have also performed direct numerical simulations to investigate the validity of our analytical predictions. In particular, we have used a high-accuracy spectral method [43] to numerically integrate the nonlocal NLS Eqs. (1)–(3), using initial conditions in the form of the dark-bright and antidark-bright soliton solutions in Eqs. (35)–(37) for $t = 0$. In both cases, the initial condition for the u-component which carries the dark or the antidark soliton (and is thus characterized by nontrivial conditions at $x, y \to \infty$) was taken to be $u(x, y, 0) = u_b(x, y)u_s(x, y, 0)$. Here, $u_s(x, y, 0)$ is the initial profile of the soliton and $u_b(x, y)$ is an almost flat background of finite extent (in the infinite system, this would be $u_b(x, y) = 1$), namely, a very broad super-Gaussian of the form $u_b(x, y) = \exp[-(x/0.8L)^{12} - (y/0.8L)^{12}]$, where $x, y \in [-L, L]$; here, L denotes the size of the computational domain, taken to be sufficiently large (e.g., of the order of 10^3). Notice that the use of a background of finite extent is more realistic, since dark (or antidark) solitons are always created on top of a finite background in real experiments (see, e.g., Ref. [23]).

As discussed above, the type of the vector soliton depends on the sign of the amplitude A, which in turn is controlled by the sign and magnitude of α. In the simulations, we fixed $d_1 = 2d_2 = g_1 = g_2 = q = 8\nu = 1$ and $d_1 = 2d_2 = g_1 = -g_2 = q = 8\nu/3 = 1$ for the case of dark-bright and antidark-bright solitons, respectively. This choice leads to a background density $\rho_0 = 1$. Furthermore, dark-bright (antidark-bright) solitons are characterized by $\alpha = 1/2$ ($\alpha = -1/2$), and amplitudes $A = 1/2$ ($A = -1/2$). Other parameter values that were used [or found consistently from our analysis—see, e.g., Eq. (33)] are as follows: $K_X = \sqrt{2}$, $K_Y = 1$,

$k_y = \sqrt{2}$, as well as $c = \sqrt{2}$ and $n_0 = 1$. Finally, $k_x = -2\sqrt{2}$ and $B = 1/\sqrt{2}$ ($B = 1$) for the dark-bright (antidark-bright) soliton.

Regarding the choice of the signs of g_1 and g_2, it is clear that dark-bright solitons exist when the nonlinearities of both components are of the defocusing type, while antidark-bright solitons exist when the component carrying the antidark (bright) soliton features a defocusing (focusing) nonlinearity.

The above parameter values lead to initial conditions, expressed in terms of the original variables and a sole free parameter, namely, the small parameter ϵ. In particular, for the dark-bright soliton, we get

$$u(x,y,0) = \left[1 - \frac{1}{2}\epsilon\,\mathrm{sech}^2(\epsilon^{1/2}\sqrt{2}x + \epsilon y)\right]^{1/2} \times \exp\left[-\frac{i}{2}\epsilon^{1/2}\tanh(\epsilon^{1/2}\sqrt{2}x + \epsilon y)\right], \quad (38)$$

$$v(x,y,0) = \frac{1}{\sqrt{2}}\epsilon\,\mathrm{sech}(\epsilon^{1/2}\sqrt{2}x + \epsilon y) \times \exp\left[-i(2\sqrt{2} + \epsilon^{1/2})x + i\sqrt{2}\left(1 + \frac{\epsilon}{4}\right)y\right], \quad (39)$$

$$n(x,y,0) = 1 - \frac{1}{2}\epsilon\,\mathrm{sech}^2(\epsilon^{1/2}\sqrt{2}x + \epsilon y), \quad (40)$$

while for the antidark-bright soliton, we have

$$u(x,y,0) = \left[1 + \frac{1}{2}\epsilon\,\mathrm{sech}^2(\epsilon^{1/2}\sqrt{2}x + \epsilon y)\right]^{1/2} \times \exp\left[\frac{i}{2}\epsilon^{1/2}\tanh(\epsilon^{1/2}\sqrt{2}x + \epsilon y)\right], \quad (41)$$

$$v(x,y,0) = \epsilon\,\mathrm{sech}(\epsilon^{1/2}\sqrt{2}x + \epsilon y) \times \exp\left[i(2\sqrt{2} - \epsilon^{1/2})x + i\sqrt{2}\left(1 + \frac{\epsilon}{4}\right)y\right], \quad (42)$$

$$n(x,y,0) = 1 + \frac{1}{2}\epsilon\,\mathrm{sech}^2(\epsilon^{1/2}\sqrt{2}x + \epsilon y). \quad (43)$$

In both cases, we have used the value $\epsilon = 0.1$. Figures 1 and 2 present results for the dark-bright and antidark-bright solitons, respectively, depicting three-dimensional plots of the initial conditions (top panels) and contour plots, showing the evolution of the solutions' modulus (bottom panels). As seen, both soliton pairs remain stable, traveling undistorted with a constant velocity, up to $t = 50$, in excellent agreement with our analytical predictions.

To test the validity of our analytical approximations, we may compare the numerical and analytical values of the solitons' velocities. For instance, in the case of the dark-bright soliton, the numerically obtained soliton velocity $v_{\rm num}$ can be found by the equation

$$v_{\rm num} = \frac{\Delta x}{\Delta t}\cos\left[\tan^{-1}\left(\frac{\tilde{K}_Y}{\tilde{K}_X}\right)\right], \quad (44)$$

where $\tilde{K}_X = (2\epsilon)^{1/2}$ and $\tilde{K}_Y = \epsilon$, i.e., $\tilde{K}_Y/\tilde{K}_X = (\epsilon/2)^{1/2}$, while Δx is the distance (in x) traveled by the soliton in time Δt. Using $\Delta x/\Delta t \approx 1.346$, as found from the simulations, as well as $\epsilon = 0.1$, we obtain $v_{\rm num} \approx 1.313$. However, the analytical prediction for the soliton velocity, $v_{\rm an}$, is

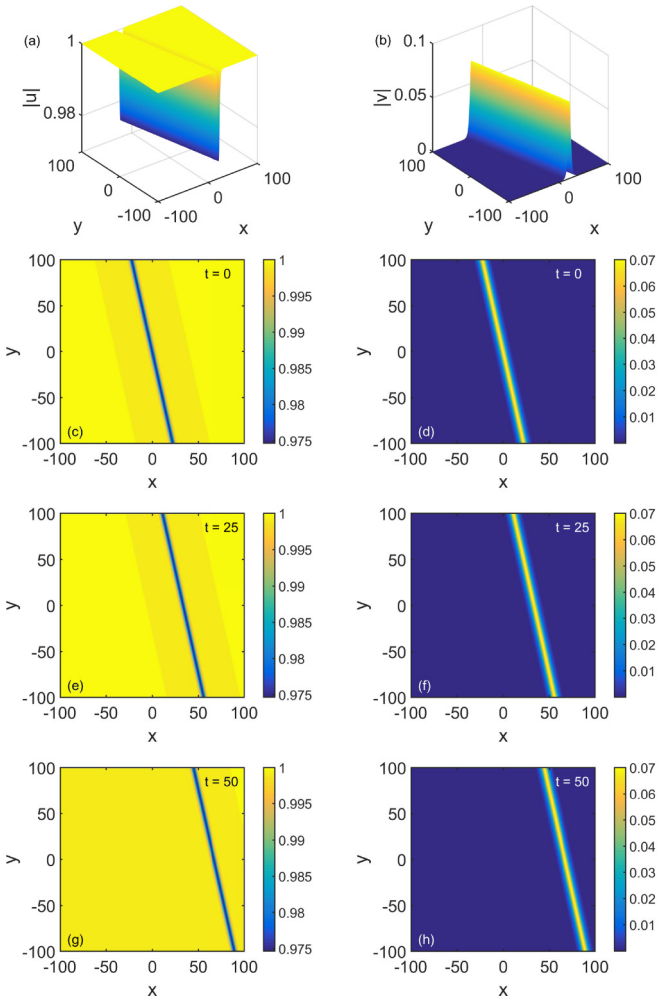

FIG. 1. The initial condition, $t = 0$ (top panels), and the time evolution, up to $t = 50$ (bottom panels), of a dark-bright soliton pair; left (right) panels correspond to the dark (bright) soliton component. The initial condition shown in the top panels is given by Eqs. (38)–(40), for $\epsilon = 0.1$.

$$v_{\rm an} = \frac{\tilde{\Omega}}{|\tilde{K}|}, \quad (45)$$

where $|\tilde{K}| \equiv \sqrt{\tilde{K}_X^2 + \tilde{K}_Y^2} = [\epsilon(\epsilon+2)]^{1/2}$ and the parameter $\tilde{\Omega}$ results from the soliton solution as: $\tilde{\Omega} = \epsilon^{1/2}(2-\epsilon)$. Using $\epsilon = 0.1$, we find $v_{\rm an} = 1.311$, which is in excellent agreement with the numerical result.

Similar results were obtained for larger values of ϵ, up to $\epsilon \approx 0.5$ (results not shown here), showing that our analytical approach is even able to describe soliton pairs of moderate amplitudes. Nevertheless, in this case, solitons are destroyed, via emission of radiation, showing smaller lifetimes. This effect can not be captured by our analytical approach which is valid only for sufficiently small values of ϵ. The effects these values play and the general instability dynamics of these solitons are further analysed below.

Furthermore, we also investigated the role of nonlocality on the evolution of the vector solitons. We found that,

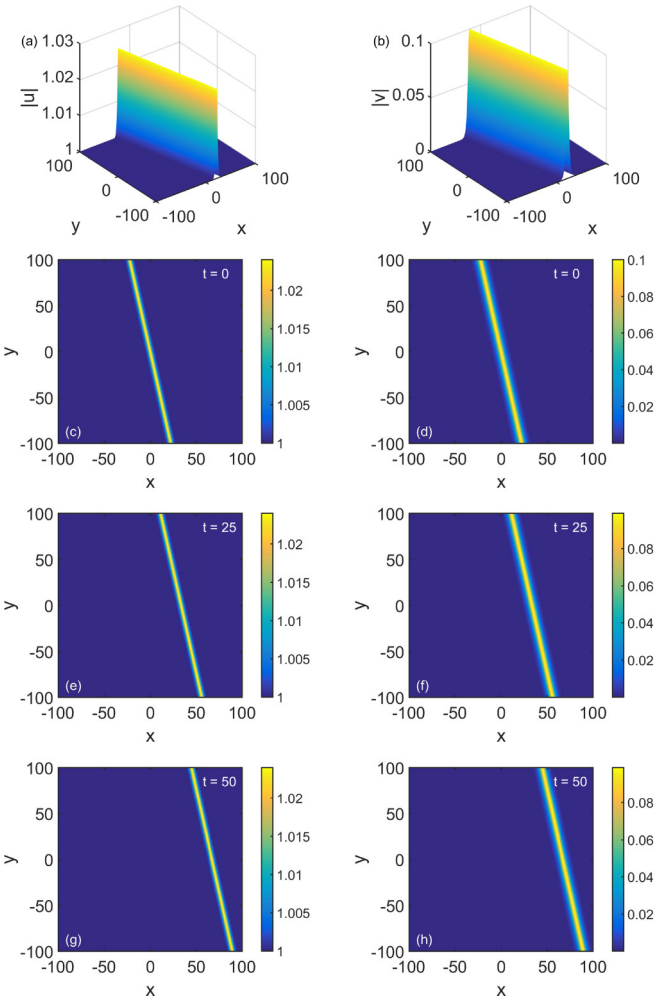

FIG. 2. Similar to Fig. 1, but now for a antidark-bright soliton pair; left (right) panels correspond to the antidark (bright) soliton component. In this case, the initial condition shown in the top panels is given by Eqs. (41)–(43), again for $\epsilon = 0.1$.

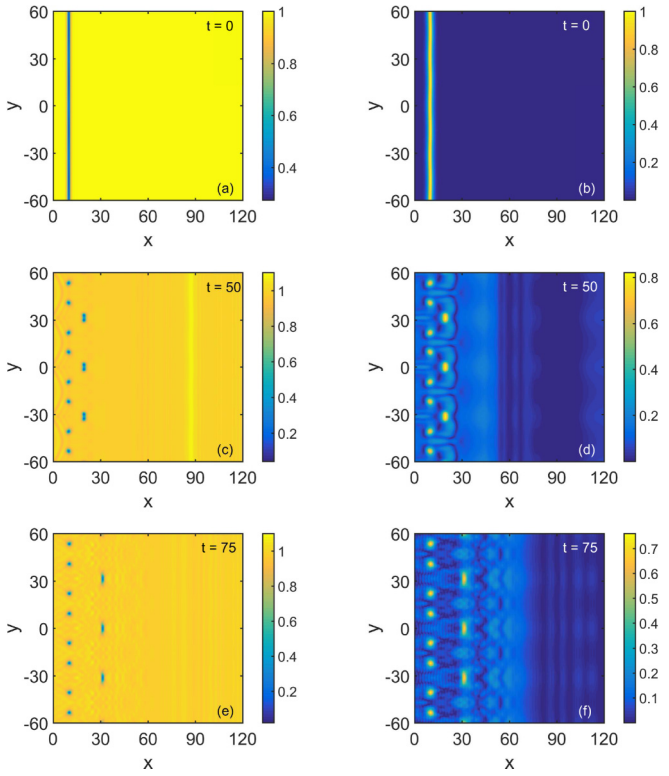

FIG. 3. Contour plots showing the evolution of the spatial profiles of the perturbed dark-bright solitons' moduli for $\nu = 1$ (close to the local NLS limit). Shown are the profiles at $t = 0$ (initial condition, top panels), $t = 50$ (middle panels), and $t = 75$ (bottom panels). Left (right) panels depict the modulus of the dark (bright) soliton component. The dark-bright solitons decay into 2D waveforms, as observed in the middle and bottom panels.

for values of ν of order $O(1)$, qualitatively similar results were obtained, while if ν becomes significantly larger, then it obviously attains a scale in terms of ϵ, and the perturbation theory fails; in this case, the vector solitons of the analytically found form of Eqs. (35)–(37) decay faster to radiation. However, close to the local limit (i.e., for small ν), we found that dark-bright solitons do exist and evolve according to our analytical predictions (see discussion in the end of Sec. III), while antidark-bright ones—which are *not* supported in the local limit—are almost immediately destroyed.

To further investigate the dynamics and stability properties of the dark-bright and antidark-bright solitons in the 2D setting, we have also performed simulations where the initial states were transversely perturbed. This is done to establish connections with well-known results regarding the transverse instability of NLS soliton stripes in the 2D setting (see, e.g., the review Ref. [44] for scalar settings, as well as Refs. [45–47] for works in multicomponent systems). We have thus used the following initial condition, corresponding to a dark- bright soliton located along the y direction, and traveling along the x direction:

$$u = \sqrt{1 - w^2}\tanh(\sqrt{1 - w^2}x) + iw, \tag{46}$$

$$v = v_0 + \delta v_{0x}\cos(\kappa_0 y), \tag{47}$$

where u is the dark soliton component, on top of a background of unit amplitude, and v is the bright soliton component. Here, w and $1 - w^2$ denote the dark soliton velocity and amplitude, respectively [with $\epsilon A = 1 - w^2$, as per Eq. (35)]. Furthermore, we have assumed that w is modulated along the transverse (y) direction as: $w = w_0[1 + \delta\cos(\kappa_0 y)]$, where w_0 and δ are the unperturbed value of w and the modulation strength, respectively, and κ_0 is the perturbation wave number. Furthermore, regarding the bright soliton component, we have used $v_0 = b\,\mathrm{sech}(bx)\exp(iw_0 x)$, with b being the inverse soliton width. In the simulations, we used the following parameter values: $w_0 = 0.3$, $\delta = 0.1$, $\kappa_0 = 3$, and $b = 0.9$. A similar initial condition was also used for the antidark-bright soliton pair, namely,

$$u = \sqrt{1 - w^2}\,\mathrm{sech}(\sqrt{1 - w^2}x) + iw, \tag{48}$$

$$v = b\,\mathrm{sech}(bx)\exp(iwx), \tag{49}$$

where u (v) denotes the antidark (bright) soliton component.

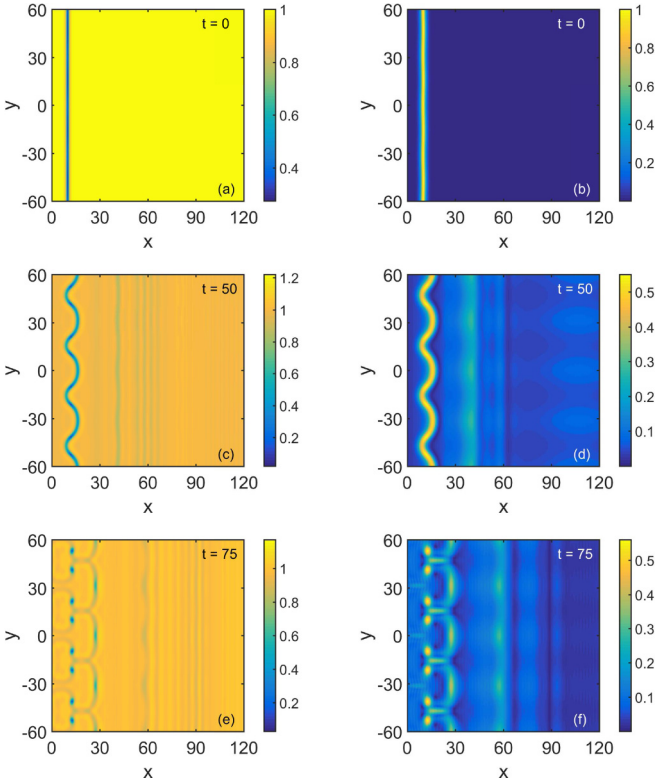

FIG. 4. Similar to Fig. 3, but for the case $\nu = 10$ (stronger nonlocality). Notice that, for $t = 50$, although the stripes undergo a rather strong undulation, they have not decayed as was the case of the weaker nonlocality. However, in this case too, the dark-bright solitons eventually decay into 2D structures.

First, we present results pertaining to dark-bright solitons. To investigate the role of nonlocality, we have performed simulations for two different values of the nonlocality parameter: for $\nu = 1$, corresponding to a weaker nonlocality [close to the local NLS limit—see Eqs. (4) and (5)], and for $\nu = 10$, corresponding to a stronger nonlocality. Corresponding results are shown in Figs. 3 and 4, respectively. It is observed that, in both cases, the solitons are prone to transverse instability and eventually decay. It is worth noticing, however, that nonlocality can partially suppress the instability; indeed, comparing Figs. 3 and 4, it is seen that, at time $t = 50$, the dark-bright soliton pair has already destroyed in the case $\nu = 1$, while for $\nu = 10$ undergoes a strong undulation, but they have not decayed yet.

It is also relevant to focus on the structures emerging from the onset of the transverse instability. As seen in both Figs. 3 and 4, and as expected from relevant theoretical results for the local NLS [44], the dark soliton stripe decays into a chain of 2D structures, which are vortex-antivortex pairs (oppositely charged vortices). This can be readily verified in the left panels of Fig. 5, showing a zoom of the modulus (top) and phase (bottom) of the dark component, at $t = 100$, in the case of $\nu = 10$. The 2D density dips, and especially the phase profile, which is characteristic of a vortex-antivortex pair, justify, indeed, the formation of vortex pairs in the dark soliton component. However, the associated bright soliton component, shown in the right panels of Fig. 5, is obviously

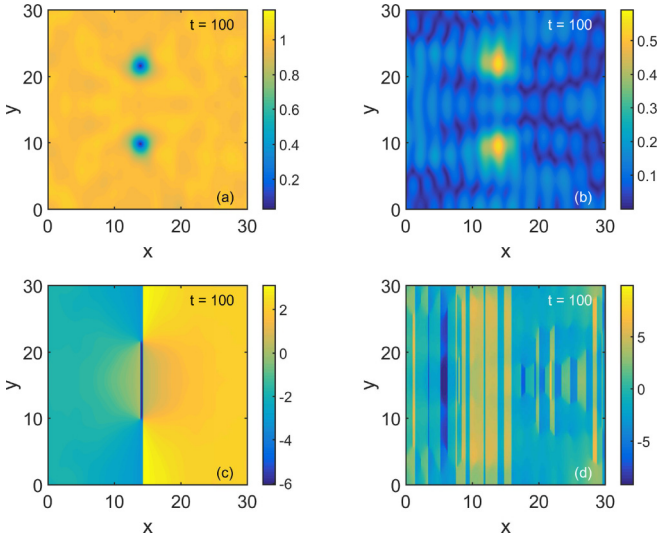

FIG. 5. Similar to Fig. 4, but for $t = 100$, where a zoom depicting the density (top panels) and phase (bottom panels) of a pair of 2D structures is shown. Left (right) panels correspond to the dark (bright) soliton components. The observed state has the form of a filled vortex pair.

a vorticity-free 2D structure which "fills" the vortex in the dark component. This filled vortex state is reminiscent to a vortex-bright soliton structure that has been predicted to occur

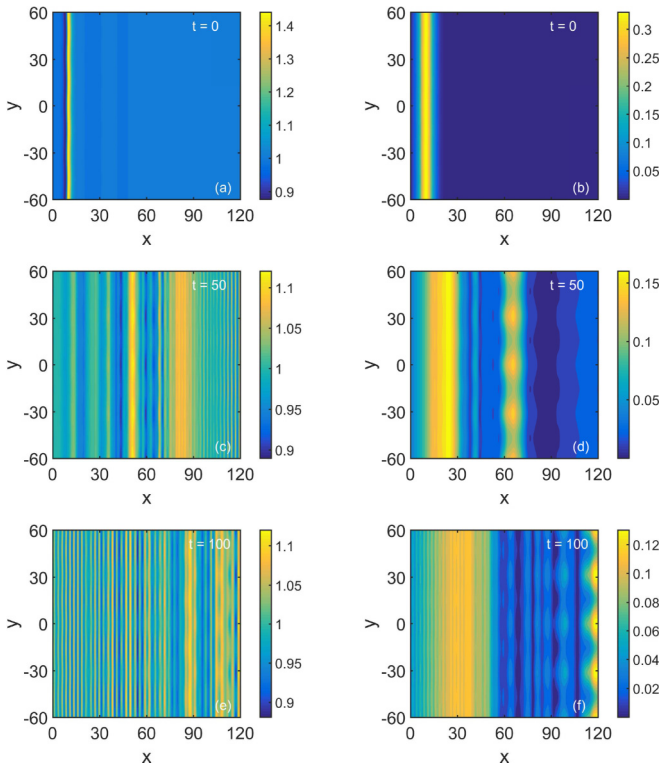

FIG. 6. Similar to Fig. 4, but for a perturbed antidark-bright soliton pair (for $\nu = 10$)—see text. In this case, the solitons decay to radiation and the instability does not give rise to the formation of 2D structures.

in two-component BECs [48] (see also the review Ref. [7] and references therein).

Hence, we can infer that relatively large-amplitude dark-bright soliton stripes decay, as a result of the onset of transverse instability, into filled vortex-antivortex pairs—or a chain of vortex-bright solitons. Nevertheless, this is not the case with antidark-bright solitons. Indeed, as shown in Fig. 6, perturbed such states are eventually destroyed, via decay into radiation, under the action of the perturbation.

V. CONCLUSIONS

In conclusion, we have studied the formation and dynamics of vector soliton stripes in a two-component 2D nonlocal NLS model. The considered model describes the interaction between two incoherently coupled optical beams, of different wavelengths, in nonlocal settings such as thermal media, plasmas, and nematic liquid crystals. We have employed a multiscale expansion method to find solutions which asymptote to a continuous wave background in the one component, and to the trivial solution in the other component. We have thus derived an integrable system in 2D, namely, the Mel'nikov system, which was introduced some time ago to describe the interaction between a long wave and a short wave packet.

The soliton solutions of the Mel'nikov system were then used for the construction of approximate vector soliton solutions of the original nonlocal NLS model. These solutions turned out to be of two different types: dark-bright soliton stripes and antidark-bright ones, which are supported in the system featuring, respectively, defocusing-defocusing or a defocusing-focusing nonlinearity in each of the two components; the latter being unique to the nonlocal system, with no counterpart in the local case. We have also performed direct numerical simulations to test the validity of our analytical approach and also study the dynamics of the obtained soliton states. We found that small-amplitude states of both types are indeed supported by the system, as it was shown that they propagate undistorted with a constant velocity, which was analytically predicted quite accurately. However, large-amplitude solitons turned out to be unstable and, typically, decay into radiation.

We have also studied the transverse instability of the derived vector soliton states. It was found that both dark-bright and antidark-bright solitons are prone to the transverse instability, with the nonlocality only partially arresting it: the onset of the instability takes place at later times in the case where nonlocality is stronger. We have also found that the transverse instability of dark-bright solitons, results in the formation of filled vortex states—reminiscent to vortex-bright solitons that were predicted to occur in two-component Bose-Einstein condensates. However, perturbed antidark-bright solitons were always found to decay into radiation.

Our analysis and results pave the way for a number of interesting future investigations. For instance, it would be interesting to investigate if other, quasi one-dimensional states—having, e.g., the form of ring solitons (see, e.g., Ref. [49])—or purely 2D soliton states, such as lumps (see, e.g., Ref. [50]) can be supported in multi-component nonlocal media. Such investigations are currently in progress, and relevant results will be reported elsewhere.

[1] T. Dauxois and M. Peyrard, *Physics of Solitons* (Cambridge University Press, cambridge, UK, 2006).

[2] M. J. Ablowitz, *Nonlinear Dispersive Waves: Asymptotic Analysis and Solitons* (Cambridge University Press, Cambridge, UK, 2011).

[3] Y. S. Kivshar and G. P. Agrawal, *Optical Solitons: From Fibers to Photonic Crystals* (Academic Press, San Diego, CA, 2003).

[4] Y. S. Kivshar and B. Luther-Davies, Phys. Rep. **298**, 81 (1998).

[5] F. Dalfovo, S. Giorgini, L. P. Pitaevskii, and S. Stringari, Rev. Mod. Phys. **71**, 463 (1999).

[6] P. G. Kevrekidis, D. J. Frantzeskakis, and R. Carretero-González, *The Defocusing Nonlinear Schrödinger Equation: From Dark Solitons to Vortices and Vortex Rings* (SIAM, Philadelphia, PA, 2015).

[7] P. G. Kevrekidis and D. J. Frantzeskakis, Rev. Phys. **1**, 140 (2016).

[8] E. Infeld and G. Rowlands, *Nonlinear Waves, Solitons and Chaos* (Cambridge University Press, Cambridge, UK, 1990).

[9] A. Alberucci, M. Peccianti, G. Assanto, A. Dyadyusha, and M. Kaczmarek, Phys. Rev. Lett. **97**, 153903 (2006).

[10] S. Trillo, S. Wabnitz, E. M. Wright, and G. I. Stegeman, Opt. Lett. **13**, 871 (1988).

[11] D. N. Christodoulides, Phys. Lett. A **132**, 451 (1988).

[12] Y. Lin and R.-K. Lee, Opt. Express **15**, 8781 (2007).

[13] T. P. Horikis and D. J. Frantzeskakis, Phys. Rev. A **94**, 053805 (2016).

[14] Y. S. Kivshar, Phys. Rev. A **43**, 1677 (1991).

[15] V. E. Vekslerchik, Phys. Lett. A **153**, 195 (1991).

[16] Y. S. Kivshar and V. V. Afanasjev, Phys. Rev. A **44**, R1446 (1991).

[17] D. J. Frantzeskakis, J. Phys. A: Math. Gen. **29**, 3631 (2010).

[18] D. J. Frantzeskakis, Phys. Lett. A **285**, 363 (2001).

[19] W. Yu, W. Liu, H. Triki, Q. Zhou, A. Biswas, and M. R. Belić, Nonlinear Dyn. **97**, 471 (2019).

[20] I. Danaila, M. A. Khamehchi, V. Gokhroo, P. Engels, and P. G. Kevrekidis, Phys. Rev. A **94**, 053617 (2016).

[21] H. Kiehn, S. I. Mistakidis, G. C. Katsimiga, and P. Schmelcher, Phys. Rev. A **100**, 023613 (2019).

[22] P. G. Kevrekidis, H. E. Nistazakis, D. J. Frantzeskakis, B. A. Malomed, and R. Carretero-González, Eur. Phys. J. D **28**, 181 (2004).

[23] J. Guo, X. Hu, Y. F. Song, G. D. Shao, L. M. Zhao, and D. Y. Tang, Phys. Rev. A **99**, 061802(R) (2019).

[24] D. Suter and T. Blasberg, Phys. Rev. A **48**, 4583 (1993).

[25] C. Rotschild, O. Cohen, O. Manela, M. Segev, and T. Carmon, Phys. Rev. Lett. **95**, 213904 (2005).

[26] N. Ghofraniha, C. Conti, G. Ruocco, and S. Trillo, Phys. Rev. Lett. **99**, 043903 (2007).

[27] C. Conti, A. Fratalocchi, M. Peccianti, G. Ruocco, and S. Trillo, Phys. Rev. Lett. **102**, 083902 (2009).

[28] W. Krolikowski, O. Bang, N. I. Nikolov, D. Neshev, J. Wyller, J. J. Rasmussen, and D. Edmundson, J. Opt. B: Quantum Semiclass. Opt. **6**, S288 (2004).

[29] D. Mihalache, Rom. Rep. Phys. **59**, 515 (2007).

[30] A. G. Litvak, V. A. Mironov, G. M. Fraiman, and A. D. Yunakovskii, Sov. J. Plasma Phys. **1**, 60 (1975).
[31] A. I. Yakimenko, Y. A. Zaliznyak, and Y. S. Kivshar, Phys. Rev. E **71**, 065603(R) (2005).
[32] M. Peccianti and G. Assanto, Phys. Rep. **516**, 147 (2012).
[33] G. Assanto, *Nematicons: Spatial Optical Solitons in Nematic Liquid Crystals* (Wiley, New York, NY, 2012).
[34] B. D. Skuse and N. F. Smyth, Phys. Rev. A **79**, 063806 (2009).
[35] T. Lahaye, C. Menotti, L. Santos, M. Lewenstein, and T. Pfau, Rep. Prog. Phys. **72**, 126401 (2009).
[36] A. Piccardi, A. Alberucci, N. Tabiryan, and G. Assanto, Opt. Lett. **36**, 1356 (2011).
[37] V. K. Mel'nikov, J. Math. Phys. **28**, 2603 (1987).
[38] V. K. Mel'nikov, Lett. Math. Phys. **7**, 129 (1983).
[39] V. K. Mel'nikov, Phys. Lett. A **118**, 22 (1986).
[40] V. K. Mel'nikov, Phys. Lett. A **128**, 488 (1988).
[41] M. Aguero, D. J. Frantzeskakis, and P. G. Kevrekidis, J. Phys. A: Math. Gen. **39**, 7705 (2006).
[42] F. Tsitoura, V. Achilleos, B. A. Malomed, D. Yan, P. G. Kevrekidis, and D. J. Frantzeskakis, Phys. Rev. A **87**, 063624 (2013).
[43] A. Kassam and L. N. Trefethen, SIAM J. Sci. Comput. **26**, 1214 (2005).
[44] Y. S. Kivshar and D. E. Pelinovsky, Phys. Rep. **331**, 117 (2000).
[45] Z. H. Musslimani, M. Segev, A. Nepomnyashchy, and Y. S. Kivshar, Phys. Rev. E **60**, R1170 (1999).
[46] Z. H. Musslimani and J. Yang, Opt. Lett. **26**, 1981 (2001).
[47] D. Neshev, W. Krolikowski, D. E. Pelinovsky, G. McCarthy, and Y. S. Kivshar, Phys. Rev. Lett. **87**, 103903 (2001).
[48] K. J. H. Law, P. G. Kevrekidis, and L. S. Tuckerman, Phys. Rev. Lett. **105**, 160405 (2010).
[49] T. P. Horikis and D. J. Frantzeskakis, Opt. Lett. **41**, 583 (2016).
[50] T. P. Horikis and D. J. Frantzeskakis, Phys. Rev. Lett. **118**, 243903 (2017).